Sustainable Chemical Engineering
https://ojs.wiserpub.com/index.php/SCE/

Research Article

Numerical Simulation for Heat Transfer of Fluid-Granular Multiphase Flow in a Preheating Furnace

Kum-Song Ku*, Myong-Il Kim, Kwang-Chol Jong, Bok-Chol Song

Institute of Mechanics, State Academy of Sciences, Pyongyang, Democratic People's Republic of Korea
E-mail: kks1970@star-co.net.kp

Received: 5 May 2025; **Revised:** 4 July 2025; **Accepted:** 8 July 2025

Abstract: In this paper, numerical simulations are carried out for the heat transfer of granular multiphase flow in a preheating furnace. In the preheating furnace hot air passes through a granular medium with a large particle size (> 1 cm) moving in a packed bed state. Here, a granular medium with a large particle size was considered as one with unilateral incompressibility. This method differs from the Eulerian method based on kinetic theory for granular flow. Also, the calculation of the thermal conductivity in packed bed of granular material used in the discrete element method was modified to fit the continuum model. To verify the validity of the combination of this heat conduction model and the Eulerian granular flow model based on the unilateral incompressibility, the comparison with the previous results using the discrete element method was done. The comparison showed a good agreement of the temperature distribution with time. Finally, this was applied to analyzing heat transfer in a preheating furnace and the results were compared with the measured temperatures of the discharged granular material in different conditions. The results show that the method based on the assumption of unilateral incompressibility is more suitable than the kinetic theory-based model for the analysis of heat transfer processes in granular flows with large particle sizes and dense particles that are not well entrained in fluid flow. The calculations show that the inlet charging rate should be less than 0.55 kg/s and the blast velocity higher than 100 m/s to achieve the discharged material temperature above 1,000 ℃. Also it was found that there exists a thin transition layer with a sharp temperature change at the free surface of the granular layer in the range of blast velocities (50 m/s～125 m/s) and granular material charging rates (0.28 kg/s～1.11 kg/s) considered here.

Keywords: computational fluid dynamics, multiphase flow, preheating furnace, discrete element method, granular flow, heat transfer

Nomenclature

Cp_s	Specific heat of granular material (J/kg·K)
d_s	Particle diameter (m)
E^*	Young's modulus of granular material (pascal)
$\mathbf{F}_{fs}$	Interaction force between fluid and the particle (N)
h_f	Enthalpy of fluid (J)
h_s	Enthalpy of granular phase (J)

DOI: https://doi.org/10.37256/sce.6220257173

H_c	Efficient heat conductivity between two particles (W/m·K)
h_i	Smoothing length (m)
h_{sf}	Heat transfer coefficient between fluid and granular material (W/m^2·K)
k_s	Heat conductivity of granular material (W/m·K)
n	Time-step superscript
n_s	Number of particles per unit volume (1/m^3)
p	Static pressure of fluid (N/m^2)
p_i	Solid pressure in ith element (N/m^2)
p_s	Solid pressure (N/m^2)
Re_i	Reynolds number of ith particle
r^*	Geometric average of particle diameters (m)
T_f	Temperature of fluid (K)
T_i	Temperature of ith particle (K)
T_s	Temperature of granular phase (K)
$\boldsymbol{u}_f$	Velocity of fluid (m/s)
$\boldsymbol{u}_s$	Velocity of granular phase (m/s)
$\boldsymbol{u}_{s,f}$	Velocity of granular phase at face f (m/s)
V_i	Volume of a particle (m^3)
W	Smoothing function
Δt	Time-step (s)
μ_s	Granular viscosity (N·s/m^2)
μ_{fr}	Frictional viscosity (N·s/m^2)
μ_{col}	Collisional viscosity (N·s/m^2)
ρ_f	Density of fluid (kg/m^3)
ρ_s	Density of granular material (kg/m^3)
σ_k	Turbulent Prandtl number for k
σ_ε	Turbulent Prandtl numbers for ε
$\boldsymbol{\tau}_f$	Viscous stress of fluid (N/m^2)
$\boldsymbol{\tau}_s$	Granular stress (N/m^2)
φ	Porosity
φ_{max}	Maximum packing limit
φ_s	Solid volume fraction
$\varphi_{s,f}$	Volume fraction of granular phase at face f
ϕ	Internal frictional angle (°)
Δ_i	Nabla operator at element i

1. Introduction

The motion of granular materials is the commonplace phenomena in the industrial processes including motion of charging materials in the furnaces or rotary kilns. Here charging material, being not pulverized, is not completely suspended in the fluid and moves in a layer. On the other hand, it can be floated in some regions where the velocity of the fluid is large. Thus the motion of system composed of large quantity of mesoscopic particles shows unique physical behavior that is unlike motion of the pulverized materials in fluid.

For decades, the study of the behaviors of these systems has interested many researchers. In particular, Discrete Element Method (DEM), one of Lagrangian methods, has been widely used to study granular flows.[1-8] In DEM, Newton's momentum equations are solved to determine the motion of every granular particle. These results can then be coupled with a set of equations for fluid flow to study the interaction with fluid. This method has advantage over Eulerian method in that it can consider shape of particles, translation or rotation of particles that come in contact with one another as well as those that do not.

Numerous examples using DEM can be found, including thermal transfer in granular flow as well as feeding in the kilns and furnaces.[9-12]

In DEM the heat transfer may be formed by two processes: heat transfer by motion of granular particles and heat conduction by contact between them. The former can be found from the solution of Newton's momentum equations for the particles because particle's thermal property (temperature) is carried by its velocity. Therefore, the study for heat transfer in DEM has focused on finding how the heat transfer by contact between particles varies with the motion state of granular packed bed.[13-18]

In granular flows the heat transfer by contact between particles differs from that by conduction within particle itself. Chaudhuri et al.[13] and Nguyen et al.[15] suggested a simple relationship expressing the effective heat conductivity by contact between particles. Mehdi et al.[19] simulated the temperature change and melting process of ice granular particles in water by using eXtended DEM (XDEM).

Guo et al.[20-23] also studied heat transfer in gravity-driven granular flow in moving bed heat exchangers for solar energy utilization.

Although DEM can effectively describe granular particle motion by utilizing a Lagrangian approach and considering the interactions resulting from the collision between particles, it requires enormous computational effort to consider the contact between particles. A new generic hierarchical approach has been proposed, sequentially combining 2D DEM simulations of slices of the bed and 3D two-phase Computational Fluid Dynamics (CFD) models of the entire kiln, encompassing both bed and gaseous freeboard.[24]

Several other works studied heat transfer characteristics in granular materials considering it as a continuum. For example, Natarajan et al.[25] suggested also the kinetic theory of heat transfer in granular flows and Zhang et al.[26] gave thermal conductivity in non-uniform granular flow.

But in many engineering applications such as rotary kiln or blast furnace, heat transfer between granular particles and surrounding gas may be necessary. Here there are mainly two approaches to solve these problems, Eulerian-Lagrangian approach and Eulerian-Eulerian approach, in which motion of primary phase is always represented by Eulerian approach.

In the Eulerian-Lagrangian approach, the motion of fluid is described by the Eulerian momentum equations, while DEM is used only for the granular phase. Then, momentum and heat exchanges between fluid and granular phase are considered to get a complete system solution.[4]

In the Eulerian-Eulerian method, the motion of the particles as well as fluid is governed by Eulerian equations as a granular system itself is also considered to be a continuum.[27-29] Here constitutive relations for the granular system are required to study a granular system in addition to mass, momentum and energy equations. There are many constitutive relations for solid pressure and stress due to collision and friction between particles.[30-33] Also, there are several applications including granular flow in a fluidized bed.[27,29,34,35] These relations seem to give good results for the pulverized granular particles but not for one with a large Stokes number. For this issue Narain et al.[36] gave a novel approach. They assumed that granular material had the unilateral incompressibility instead of a constitutive relationship and then reduced it to an optimization problem for solid pressure and stresses. In our previous study,[37] their method was also adopted for granular flow with a large Stokes number.

Tyliszczak et al.[38] presented a novel computational algorithm for modeling of heat and mass transfer processes around neighboring solid objects and inside granular layers. Philipp et al.[39] also proposed a continuous model approach, based on the theory of soil mechanics to describe the granular flow inside the heat exchanger.

The present study gives the results of numerical simulation of the temperature distribution in a preheating furnace. In the preheating furnace, the particles are not fluidized as in the fluidized bed because of the large particle size (> 1 cm) and the high density. Therefore, we use the unilateral incompressibility-based granular flow model[37] given in our previous work instead of the kinetic theory based granular flow model. Heat transfer by the convection in the granular materials depends on the velocity field which is found from the momentum equation for granular phase. Needless to say, finding the reasonable velocity field of granular materials is of great necessity in the calculation of heat transfer. Also solid pressure given by a new approach is included in energy equation for the granular phase influencing the thermal distribution. Once again, our previous approach used the unilateral incompressibility assumption instead of kinetic theory based model for the granular materials. Therefore, the first object of this study is to test whether our previous approach can be fitted to calculation of convective heat transfer in the granular flow. In this paper, it is found

that for the preheated furnace we consider, the heat transfer calculation method based on the one-sided incompressibility assumption is more suitable compared to the kinematic model-based method.

Next in order to calculate heat conductivity in a packed bed, the method used in DEM was modified to be fit for continuum model. This was compared with DEM results by Chaudhuri et al.[13] Finally, the flow of heated gas through packed bed in a preheating furnace was studied. Here, conduction between granular particles, heat transfer by the convection of the granular materials and heat exchange between gas and particles occurred simultaneously. Also the temperature distribution of the bed material with charging rate of the granular material, flux of the blast air and the temperature of blast air in the preheating furnace was obtained by numerical simulation.

The paper is organized as follows: In section 2 the modeling for heat transfer in granular multiphase flow as well as momentum equations for phases are given. Section 3 describes discretization procedure of equations for calculating solid pressure and algorithm. In section 4 heating process of granular particles in a rotary cylinder is simulated by method presented and the result is compared with previous work to verify the correctness. Finally, heat transfer process in a preheating furnace is analyzed.

2. Mathematical models for different phases

2.1 *Governing equations*

2.1.1 *Governing equations of fluid flow*

In multiphase flow accompanying the granular materials the continuity and momentum equations for fluid flow are represented as

$$\frac{\partial}{\partial t}\left(\varphi\rho_{\mathrm{f}}\right)+\nabla\cdot\left(\varphi\rho_{\mathrm{f}}\boldsymbol{u}_{\mathrm{f}}\right)=0, \tag{1}$$

$$\frac{\partial}{\partial t}\left(\varphi\rho_{\mathrm{f}}\boldsymbol{u}_{\mathrm{f}}\right)+\nabla\cdot\left(\varphi\rho_{\mathrm{f}}\boldsymbol{u}_{\mathrm{f}}\boldsymbol{u}_{\mathrm{f}}\right)=-\varphi\nabla p+\nabla\cdot\varphi\boldsymbol{\tau}+\varphi\rho_{\mathrm{f}}\mathbf{g}+\mathbf{F}_{\mathrm{sf}}, \tag{2}$$

where t is the time, φ the porosity and ρ_{f}, p, $\boldsymbol{\tau}$ and $\boldsymbol{u}_{\mathrm{f}}$ are the density, pressure, viscous stress and velocity of fluid, respectively, and $\mathbf{F}_{\mathrm{sf}}$ is momentum source due to interaction between fluid and granular particles.

As the turbulence model for fluid flow, the $k-\varepsilon$ model is used and the equation for k and ε is given as follows:

$$\frac{\partial}{\partial t}\left(\varphi\rho_{\mathrm{f}}k\right)+\nabla\cdot\left(\varphi\rho_{\mathrm{f}}k\boldsymbol{u}_{\mathrm{f}}\right)=\nabla\cdot\left[\left(\mu_{\mathrm{f}}+\frac{\mu_{\mathrm{t}}}{\sigma_{\mathrm{k}}}\right)\varphi\nabla k\right]+\varphi G_{\mathrm{k}}+G_{\mathrm{b}}-\varphi\rho_{\mathrm{f}}\varepsilon+S_{\mathrm{k}}, \tag{3}$$

$$\frac{\partial}{\partial t}\left(\varphi\rho_{\mathrm{f}}\varepsilon\right)+\nabla\cdot\left(\varphi\rho_{\mathrm{f}}\varepsilon\boldsymbol{u}_{\mathrm{f}}\right)=\nabla\cdot\left[\left(\mu_{\mathrm{f}}+\frac{\mu_{\mathrm{t}}}{\sigma_{\varepsilon}}\right)\varphi\nabla\varepsilon\right]+\frac{\varepsilon}{k}\left(\varphi C_{1\varepsilon}G_{\mathrm{k}}-C_{2\varepsilon}\varphi\rho_{\mathrm{f}}\varepsilon+C_{3\varepsilon}G_{\mathrm{b}}\right)+S_{\varepsilon}, \tag{4}$$

where G_{k} is the generation of turbulence kinetic energy due to the mean velocity gradients, G_{b} the generation of turbulence kinetic energy due to interphase interaction, $C_{1\varepsilon}$, $C_{2\varepsilon}$ and $C_{3\varepsilon}$ are constants. σ_{k} and σ_{ε} are the turbulent Prandtl numbers for k and ε, respectively. S_{k} and S_{ε} are user-defined source terms.

Energy equation for fluid flow can be written as

$$\frac{\partial}{\partial t}\left(\varphi\rho_{\mathrm{f}}h_{\mathrm{f}}\right)+\nabla\cdot\left(\varphi\rho_{\mathrm{f}}h_{\mathrm{f}}\boldsymbol{u}_{\mathrm{f}}\right)=\varphi\frac{\partial p}{\partial t}+\boldsymbol{\tau}_{\mathrm{f}}:\nabla\boldsymbol{u}_{\mathrm{f}}-\nabla\cdot\boldsymbol{H}_{\mathrm{f}}+S_{\mathrm{f}}+Q_{\mathrm{fs}} \tag{5}$$

where h_{f} is the specific enthalpy of fluid, $\boldsymbol{H}_{\mathrm{f}}$ the heat flux due to conduction, S_{f} the source (that is here assumed to be 0)

due to chemical reaction or radiation, Q_{fs} the heat transfer term between fluid and granular particles.

2.1.2 *Governing equations of granular flow*

The equation for mass conservation in the granular flow can be written as

$$\frac{\partial}{\partial t}\left(\varphi_s \rho_s\right)+\nabla\cdot\left(\varphi_s \rho_s \boldsymbol{u}_s\right)=0, \tag{6}$$

where ρ_s and $\boldsymbol{u}_s$ are the density and velocity of granular particles, respectively, and $\varphi_s = 1 - \varphi$.

The motion of granular materials in the gas flow can be also described based on Eulerian model of multiphase flows as

$$\frac{\partial}{\partial t}\left(\varphi_s \rho_s \boldsymbol{u}_s\right)+\nabla\cdot\left(\varphi_s \rho_s \boldsymbol{u}_s \boldsymbol{u}_s\right)=-\varphi_s \nabla p-\nabla p_s+\nabla\cdot\boldsymbol{\tau}_s+\varphi_s \rho_s \mathbf{g}+\mathbf{F}_{fs}, \tag{7}$$

where p_s is solid pressure, $\boldsymbol{\tau}_s$ the stress occurred due to the motion of granular materials, and $\mathbf{F}_{fs}$ momentum source term due to interaction between fluid and granular particles.

Energy equation of granular flow can be also written as a similar form to that of fluid, which is as follows:

$$\frac{\partial}{\partial t}\left(\varphi_s \rho_s h_s\right)+\nabla\cdot\left(\varphi_s \rho_s h_s \boldsymbol{u}_s\right)=\varphi_s \frac{\partial p_s}{\partial t}+\boldsymbol{\tau}_s : \nabla \boldsymbol{u}_s-\nabla\cdot\boldsymbol{H}_s+Q_{sf}, \tag{8}$$

where $\boldsymbol{H}_s$ is heat flux due to conduction in the granular material and $Q_{sf} = -Q_{fs}$.

2.1.3 *Frictional and collisional viscosity*

Here, Schaeffer's model is used for frictional viscosity.[30,40] Therefore, frictional viscosity may be written as follows:

$$\mu_{fr}=\frac{p_s \sin\phi}{\sqrt{I_{2D}}} \tag{9}$$

where ϕ is the internal frictional angle depending on the granular particle size and material properties, and I_{2D} is the second invariant of the deviatoric stress tensor. Also p_s is solid pressure that satisfies equations (11) and (12).

The collisional viscosity may be considered similar to molecular viscosity in thermodynamics and may be written as follows:[37]

$$\mu_{col}=\beta_2 \rho_s \varphi_s^2 S_s, \quad \text{if} \quad \varphi_s < 0.99\varphi_{max},$$

$$\mu_{col}=0, \quad \text{if} \quad \varphi_s > 0.99\varphi_{max}, \tag{10}$$

where β_2 is a constant dependent upon granular particle properties and S_s is the efficient collisional cross-sectional area.

2.2 *Modelling of solid pressure*

According to Gidaspow,[41] solid pressure has been described by granular temperature in multiphase flow. This model was obtained from kinetic theory for very small particles (such as pulverized coal), and therefore is not adequate when particles have large diameter and material density is much greater than that of the fluid. In this case particle motion is not significantly affected by fluid flow. Therefore, it is not appropriate to describe granular pressure by

granular temperature, which is a thermodynamic property. When the volume fraction exceeds the packing limit for granular particles with large diameter and material density is much greater than that of the fluid, compressive pressure may be produced due to gravitational force. If granular materials are in motion at this status, friction force may give greater influence to its motion than the interaction due to collision between granular particles. Additionally, if the solid volume fraction, φ_s becomes less than the maximum packing limit, φ_{max}, the compressive pressure between particles vanishes and, at this moment, interaction force due to the collision between particles may become dominant. Namely, granular materials have unilateral incompressibility.

Because particle material density is assumed to be constant, unilateral incompressibility is described as follows:[36]

$$\varphi_s \le \varphi_{max} \tag{11}$$

or

$$p_s\left(\varphi_{max} - \varphi_s\right) = 0, \quad \text{if } p_s \ge 0. \tag{12}$$

Equation (12) implies that when a material experiences maximum packing limit, solid pressure should be nonzero, and when it is less, solid pressure should be zero.

2.3 *Momentum interaction between fluid and particles*

Many models exist for the interaction between a fluid and granular particles, such as Wen & Wu and Ergun models.[27,42,43] However, in most research based on DEM,[2,9,44] the DiFelice model has been used. In this model, the magnitude of the force applied on a particle by a fluid can be written as follows:[41]

$$\mathbf{F}_{f,i} = \mathbf{F}_{f0,i}\varphi_s^{-(\chi+1)} \tag{13}$$

where

$$\mathbf{F}_{f0,i} = 0.125 C_{d0,i}\rho_f \pi d_s^2 \varphi_s^2 \left|\boldsymbol{u}_f - \boldsymbol{u}_s\right|\left(\boldsymbol{u}_f - \boldsymbol{u}_s\right),$$

$$\chi = 3.7 - 0.65\exp\left[-\frac{\left(1.5 - \log_{10}\mathrm{Re}_i\right)^2}{2}\right],$$

$$C_{d0,i} = \left(0.63 + \frac{4.8}{\sqrt{\mathrm{Re}_i}}\right)^2,$$

$$\mathrm{Re}_i = \frac{\rho_f d_s \varphi_s}{\mu_f}\left|\boldsymbol{u}_f - \boldsymbol{u}_s\right|,$$

and ρ_f is fluid density, μ_f is fluid viscosity, and d_s is particle diameter.

Because equation (13) represents the force acting on a particle, a modification is required when applying it to Eulerian model. If the number of particles per unit volume is n_s, the total force acting on particles in a unit volume may be written as follows:

$$\mathbf{F}_{fs} = n_s \mathbf{F}_{f,i} = \frac{\varphi_s}{V_i}\mathbf{F}_{f,i}, \tag{14}$$

where $V_i = \pi d_s^3/6$ is the volume of a particle. Here, the particle was assumed to be spherical.

2.4 *Contact heat conductivity between particles*

When the diameter of particles is small, contact area between them is great, so the conductivity within packed bed is almost the same as that of granular material. However, the greater the diameters of particles, the smaller contact area between them, so heat conductivity of packed bed significantly differs from that in granular particle.

In general, in DEM heat transfer flux through the boundary between two particles *i* and *j* is expressed as

$$Q_{ij} = H_c\left(T_j - T_i\right),$$

where T_i and T_j are the temperatures of two particles, and H_c is efficient heat conductivity between two particles that is expressed as

$$H_c = 2k_s\left[\frac{3F_N r^*}{4E^*}\right]^{\frac{1}{3}} \tag{15}$$

(Chaudhuri et al.[13] and Nguyen et al.[15]).

In above equation k_s and E^* are heat conductivity and Young's modulus of granular material, respectively, and r^* geometric average of particle diameters, F_N normal force between particles which are in contact. In the continuum model, the normal force between particles is not possible, but when the medium is in a packing state, the solid pressure can be considered to represent the normal force between particles. Therefore, the normal force between particles in equation (15) is replaced with solid pressure and some coefficients are also modified slightly, resulting in the following equation:

$$H_c = 2k_s\left[\frac{\alpha p_s r}{E^*}\right]^{1/3} \tag{16}$$

where *a* is a suitable coefficient and *r* is the radius of a particle. Next, heat flux due to conduction in the granular material may be represented as

$$\boldsymbol{H}_s = H_c \nabla T_s. \tag{17}$$

This is a slight modification of heat conduction model used in DEM and is substituted into equation (8) to be used in finding final temperature field.

2.5 *Heat transfer between granular material and fluid*

Heat transfer term Q_{sf} in energy equation (8) can be written as

$$Q_{sf} = h_{sf} A\left(T_f - T_s\right) \tag{18}$$

where T_f and T_s are the temperature of fluid and granular material, respectively, A is the interfacial area between fluid and a particle. And h_{sf} is heat transfer coefficient between fluid and granular material which is represented as

$$h_{sf} = \frac{k_s Nu_s}{d_s}. \tag{19}$$

Here, Nu_s is Nusselt number to be calculated by Gunn's model,[45] which is available for the granular flows with porosities ranging from 0.35 to 1.0 and Reynolds numbers up to 10^5. In Gunn's model Nu_s is found as

$$Nu_s = \left(7 - 10\varphi_s + 5\varphi_s^2\right)\left(1 + 0.7\,\mathrm{Re}_s^{0.2}\,Pr^{\frac{1}{3}}\right) + \left(1.33 - 2.4\varphi_s + 1.2\varphi_s^2\right)\mathrm{Re}_s^{0.7}\,Pr^{1/3}, \tag{20}$$

where Pr is Prandtl number to be calculated as $Pr = Cp_s\mu_s/k_s$, Cp_s the specific heat at constant pressure, and μ_s the viscosity of granular material defined at the point of view of continuum medium.

3. Discretization of governing equations

3.1 *General discretization*

Equations (1)-(5) and equations (6)-(8) are governing equations of fluid and granular flows, respectively. They are discretized based on Finite Volume Method (FVM) and can be solved in terms of SIMPLE method well-known in CFD.[46,47] The solid pressure, p_s in equation (7) has to be determined to satisfy conditions (9) and (10). In order to calculate p_s, the following discretization step was introduced. At first, equation (6) is discretized in time as follows:

$$\varphi_s^{n+1} = \varphi_s^n - \Delta t\nabla\cdot\left(\varphi_s^{n+1/2}\boldsymbol{u}_s^{n+1/2}\right). \tag{21}$$

Dividing both sides of equation (7) by ρ_s and discretizing in time, we obtain the following expression.

$$\varphi_s^{n+1/2}\boldsymbol{u}_s^{n+1/2} = \varphi_s^n\boldsymbol{u}_s^n - \frac{\Delta t}{2}\left[\nabla\cdot\left(\varphi_s\boldsymbol{u}_s\boldsymbol{u}_s\right) + \frac{\varphi_s\nabla p}{\rho_s} - \frac{\nabla\cdot\boldsymbol{\tau}_s}{\rho_s} - \varphi_s\mathbf{g} - \frac{\mathbf{F}_{fs}}{\rho_s}\right]^n - \frac{\Delta t}{2\rho_s}\nabla p_s$$

$$= \varphi_s^n\boldsymbol{u}_s^n - \frac{\Delta t}{2}\mathbf{F}^n - \frac{\Delta t}{2\rho_s}\nabla p_s, \tag{22}$$

where

$$\mathbf{F} = \nabla\cdot\left(\varphi_s\boldsymbol{u}_s\boldsymbol{u}_s\right) + \frac{\varphi_s\nabla p}{\rho_s} - \frac{\nabla\cdot\boldsymbol{\tau}_s}{\rho_s} - \varphi_s\mathbf{g} - \frac{\mathbf{F}_{fs}}{\rho_s}. \tag{23}$$

Substituting equation (22) into equation (21) and subtracting both sides from φ_{max}, the resultant equation is written as

$$\varphi_{max} - \varphi_s^{n+1} = \varphi_{max} - \varphi_s^n + \Delta t\nabla\cdot\left(\varphi_s^n\mathbf{v}_s^n\right) - \frac{\Delta t^2}{2}\nabla\cdot\mathbf{F}^n - \frac{\Delta t^2}{2}\nabla^2 p_s. \tag{24}$$

3.2 *Discretization of $\nabla^2 p_s$*

For the discretization of $\nabla^2 p_s$ term the following discretization operator used in the Smoothed Particle Hydrodynamics (SPH) method was adopted:[48]

$$\left(\nabla^2 p_s\right)_i = \sum_j \Delta V_j \frac{p_{ij}\mathbf{r}_{ij}\nabla_i W_{ij}}{\left|\mathbf{r}_{ij}^2\right| + \delta h_i^2} \tag{25}$$

where ΔV_j is the discretized element volume, $\mathbf{r}_{ij}$ is the distance between an element and its j-th neighbor, $p_{ij} = p_i - p_j$ is the pressure difference between them. In addition, $\nabla_i W_{ij}$ is the derivative of smoothing function W at considered element and h_i is the smoothing length. δ is a constant to avoid the singularity and its value is generally 0.01. In 3D case the third order spline function is used as the smoothing function.

3.3 *Discretization of other terms*

The term $\nabla\cdot(\varphi_s \boldsymbol{u}_s)$ was discretized using Gauss integration for each element.[47]

$$\nabla\cdot\left(\varphi_s \boldsymbol{u}_s\right) = \frac{1}{|\Delta V|}\int_{\partial\Delta V} \varphi_s \boldsymbol{u}_s \cdot d\mathbf{S} \approx \sum_f \varphi_{s,f} \boldsymbol{u}_{s,f}\cdot\mathbf{S}_f = \frac{\sum_f \varphi_{s,f}\mathrm{Flux}_{s,f}}{\rho_s} \tag{26}$$

where $|\Delta V|$ is the volume size of the element ΔV being considered, $\partial\Delta V$ is the surface (boundary) of the control volume or element ΔV. Also, the subscript f in summation symbol refers to the faces enclosing the element while $\varphi_{s,f}$ and $\boldsymbol{u}_{s,f}$ are volume fraction and velocity of granular phase at face f, respectively, and $\mathbf{S}_f$ the area vector on the face. $\varphi_{s,f}$ is obtained based on upwind method from φ_s values at both elements sharing the face and $\mathrm{Flux}_{s,f}$ is face flux of granular phase which can be provided by Analysis System (ANSYS) Fluent via User-Defined Function (UDF).

Same method was used even in the discretization of convective term in equation (22), i.e.

$$\nabla\cdot\left(\varphi_s \boldsymbol{u}_s \boldsymbol{u}_s\right) = \frac{1}{|\Delta V|}\int_{\partial\Delta V} \varphi_s \boldsymbol{u}_s \boldsymbol{u}_s \cdot d\mathbf{S} \approx \sum_f \varphi_{s,f} \boldsymbol{u}_{s,f}\boldsymbol{u}_{s,f}\cdot\mathbf{S}_f = \frac{\sum_f \varphi_{s,f}\,\mathrm{Flux}_{s,f}\,\boldsymbol{u}_{s,f}}{\rho_s}. \tag{27}$$

After finding $\mathbf{F}^n$ for each element, the term $\nabla\cdot(\mathbf{F}^n)$ was discretized using the SPH method as follows:

$$\nabla\cdot\left(\mathbf{F}^n\right)_i = \sum_j \Delta V_j \left(\mathbf{F}_j^n - \mathbf{F}_i^n\right)\cdot\nabla_i W_{ij}. \tag{28}$$

Substituting the discretized equation (24) into conditions (11) and (12) allows us to formulate an optimization problem for calculating the solid pressure.[36,37]

3.4 *Boundary condition and algorithm*

A no-slip condition was applied to the wall. At the outlet where the granular material exits, the boundary condition is given so that all granular material from the top is discharged.

The algorithm is mostly the same as the previous study.[37]

Here reduced conductivity of granular materials given by equation (16) is coupled by UDF code.

It should be noted that φ_s given by equation (21) has to be used during calculation of equations (26), (27), although values given by ANSYS Fluent are used for velocity and flux. φ_s is artificially constrained not to exceed packed limit in ANSYS Fluent. Therefore if in our algorithm this value is used, calculation of p_s in equation (24) is affected.

When granular packed bed moves very slowly (velocity of the bed is less than 1 cm/s), this management make the calculation to be stable.

The algorithm is summarized as follows.

(1) Set the initial values for fluid flow and granular flow.

(2) Solve equations (1)-(8) in ANSYS Fluent using the initial values given by the SIMPLE method.

(3) Calculate φ_s from equation (21) using given velocity of the granular phase in the UDF code.

(4) Calculate p_s from equation (24) in the UDF code.

(5) Repeat steps 2-4 until the solutions converge.

4. Results and discussion

4.1 *Heat transfer of granular particles in a rotating cylinder*

At first in order to verify the validity of the model for the contact heat conductivity between particles and convective heat transfer of the particles, the heat transfer of granular particles in a rotating cylinder was simulated. In this example, heat transfer between gas and particles was not considered. The model in Chaudhuri et al.[13] is used as a computational model. The cylinder is 18 cm in diameter, 1cm in length, and each particle is 2 mm in diameter with a density of 8,900 kg/m^3. Initially, half of the cylinder is full of particles and the cylinder is rotated at a velocity ranging from 30 to 80 rpm. The temperature of cylinder wall is 1,298 K and initial temperature of granular material bed is 300 K. The computation was performed for the cases when the heat conductivity of granular material are 192.5, 272, 385 W/m·k. The number of mesh elements is 9,231.

The computation is performed by using Eulerian model of ANSYS Fluent.

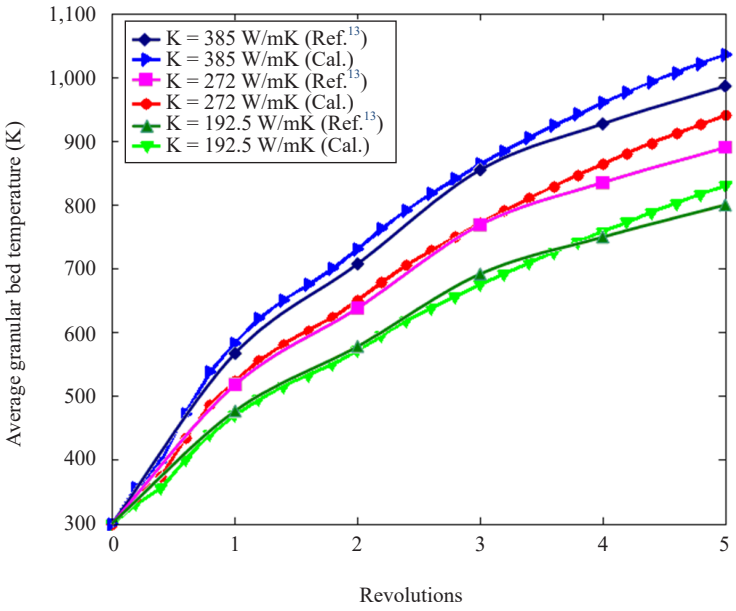

Figure 1. Average temperatures of granular material along with the revolution

Here the granular and frictional viscosity, solid pressure of secondary phase, and heat conductivity of granular material are modified by means of UDF code. Also, for the comparison with previous work the interphase convective and radiative heat transfers are not considered.

Average temperatures of granular material along with the revolution are displayed in Figure 1 to compare with the result from DEM. As shown in this figure, the present result is well consistent with one from Chaudhuri et al.[13] obtained by DEM. From this, it can be said that it is reasonable to use the solid pressure obtained based on the assumption of unilateral incompressibility in the calculation of heat transfer in the packed bed.

Figure 2 shows the temperature distributions within granular bed when heat conductivity is fixed as 385 W/m·K.

It is shown from this figure that at 1 revolution the temperatures near wall are distinct from ones far from the wall but as the revolution increases, temperature differences become small and overall average temperature becomes high because of heat conduction and mixture of particles.

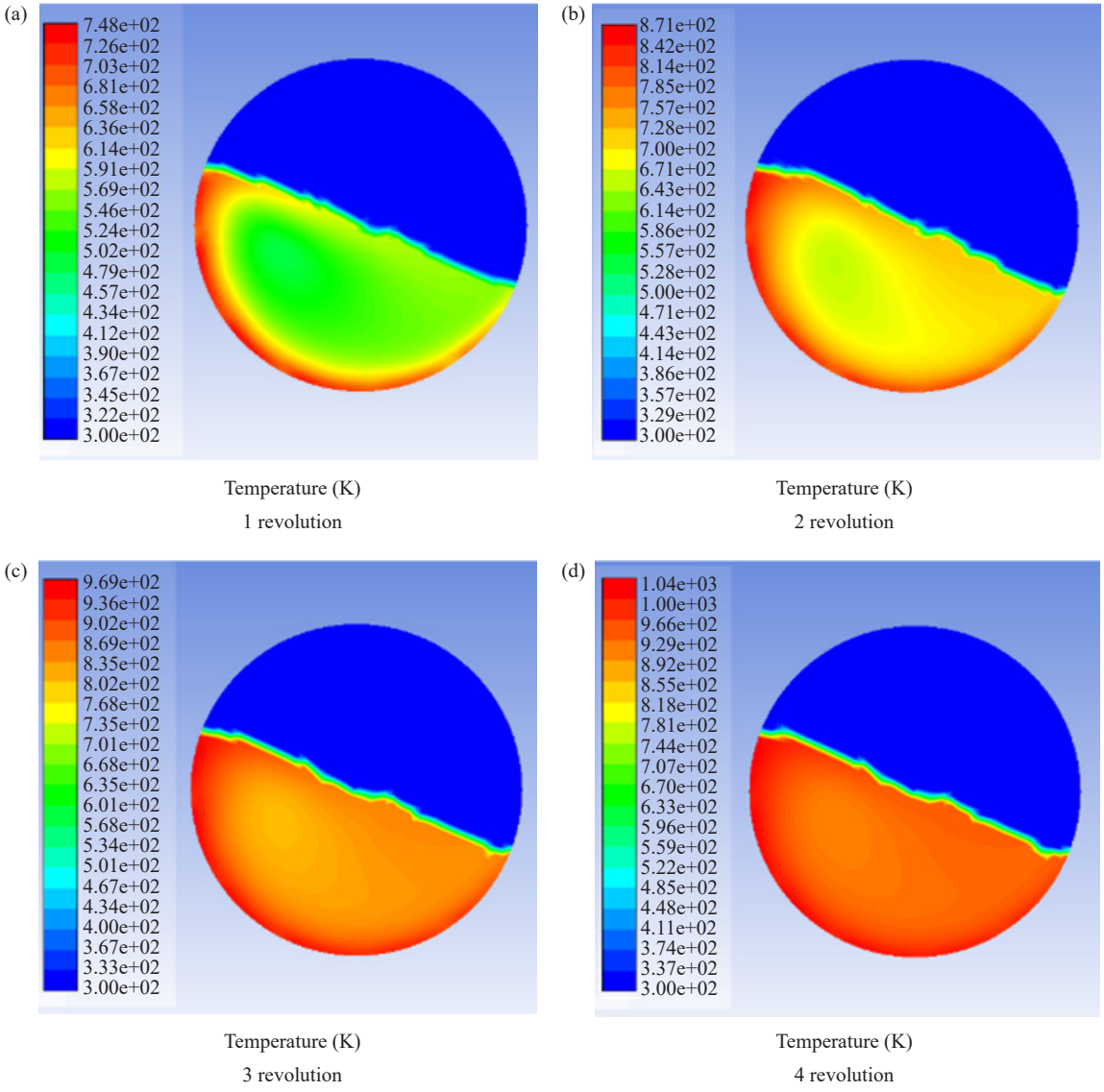

Figure 2. Temperature distributions (K) of granular bed along with the revolution when rotation velocity is 20 rpm and heat conductivity is 385 W/m·K

4.2 *Heat transfer in a preheating furnace*

In the present study both dynamic and thermal interactions between granular materials and heated gas are investigated in a preheating furnace.

Figure 3 shows geometry of model used for computation. The model is similar to that of the blast furnace which is widely used in the ironmaking industry. The study of flow characteristics in blast furnaces has already been widely conducted.[49-54] However, there is no case here that the heating process of a moving granular bed by hot gas is studied by the Eulerian approach.

The heated gas with temperature of 1,700 K is blown through tuyeres on both sides of the furnace. The feed of granular materials into the furnace was modeled by mass source of continuity equation for granular materials, which has a positive value at the elements adjacent to bottom boundary of rectangle of 0.5 m × 0.3 m surrounding it's center. In all cases, the amount of granular material discharged is equal to the amount of granular material being charged. The discharge was also modeled by the above-mentioned source, which has a negative value at the elements adjacent to bottom boundary of square of 0.3 m × 0.3 m surrounding it's center. Granular material has the density of 2,300 kg/m^3, specific heat of 856 J/kg·K, heat conductivity of 2.25 W/m·K and diameter of a particle is 2 cm. The heated gas is an

ideal gas, with a specific heat of 1,006.43 J/kg·K and a heat conductivity of 0.0242 W/m·K. The viscosity depends on the temperature according to the Sutherland's law with three coefficients. The charging rate of granular material was varied from 0.28 kg/s to 1.11 kg/s. When the charging rate of granular material changes in this range, the granular bed moves slowly at a rate less than 1 cm/s. The unsteady calculation was performed with a time step of 0.01 s until the temperature field reached steady state. The time to reach steady state is about 3,000~3,500 seconds.

At first the mesh dependence of the computational model was examined.

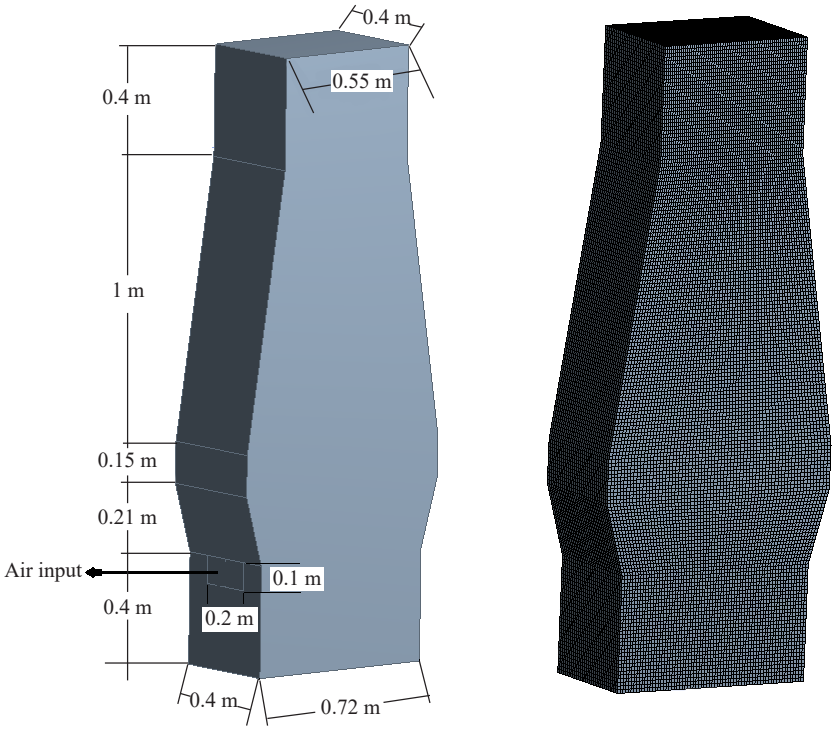

Figure 3. Dimensions and mesh of the preheating furnace

Table 1 shows the pressure loss in the furnace and the average temperature of the exhausted gas as a function of the number of mesh elements. Here the gas inlet velocity is 125 m/s, the gas temperature is 1,700 K, and charging rate of the granular material is 0.28 kg/s. The mesh is composed of hexahedral elements as shown in Figure 3. As shown in Table 1, when the mesh size is reduced from 2.5 cm to 1 cm, there is a difference in the pressure loss, but the average temperature of the exhausted gas is almost no different.

Table 1. The mesh dependence of the pressure loss in the furnace and the average temperature of the gas at the outlet

Number of elements	Mesh size (cm)	Pressure loss (Pa)	Average temperature (K)
50,400	2.5	13,201.6	1,344.13
96,320	2	13,574.1	1,346.06
243,600	1.5	13,742.7	1,348.56
393,024	1.25	13,763.2	1,348.01
767,120	1	13,765.0	1,347.43

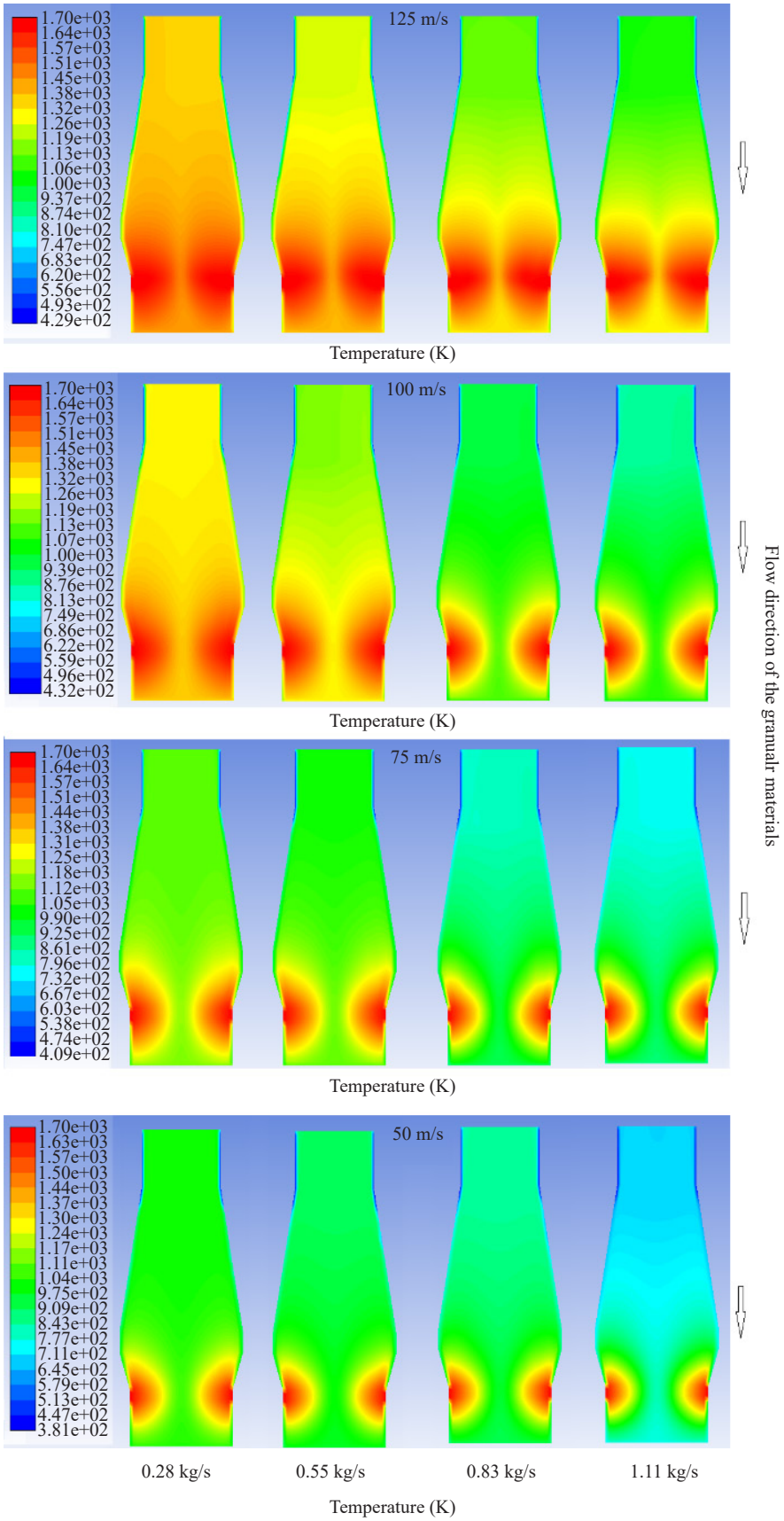

Figure 4. Temperature distribution (K) of gas phase according to the charging rate and blast velocity on the central vertical section

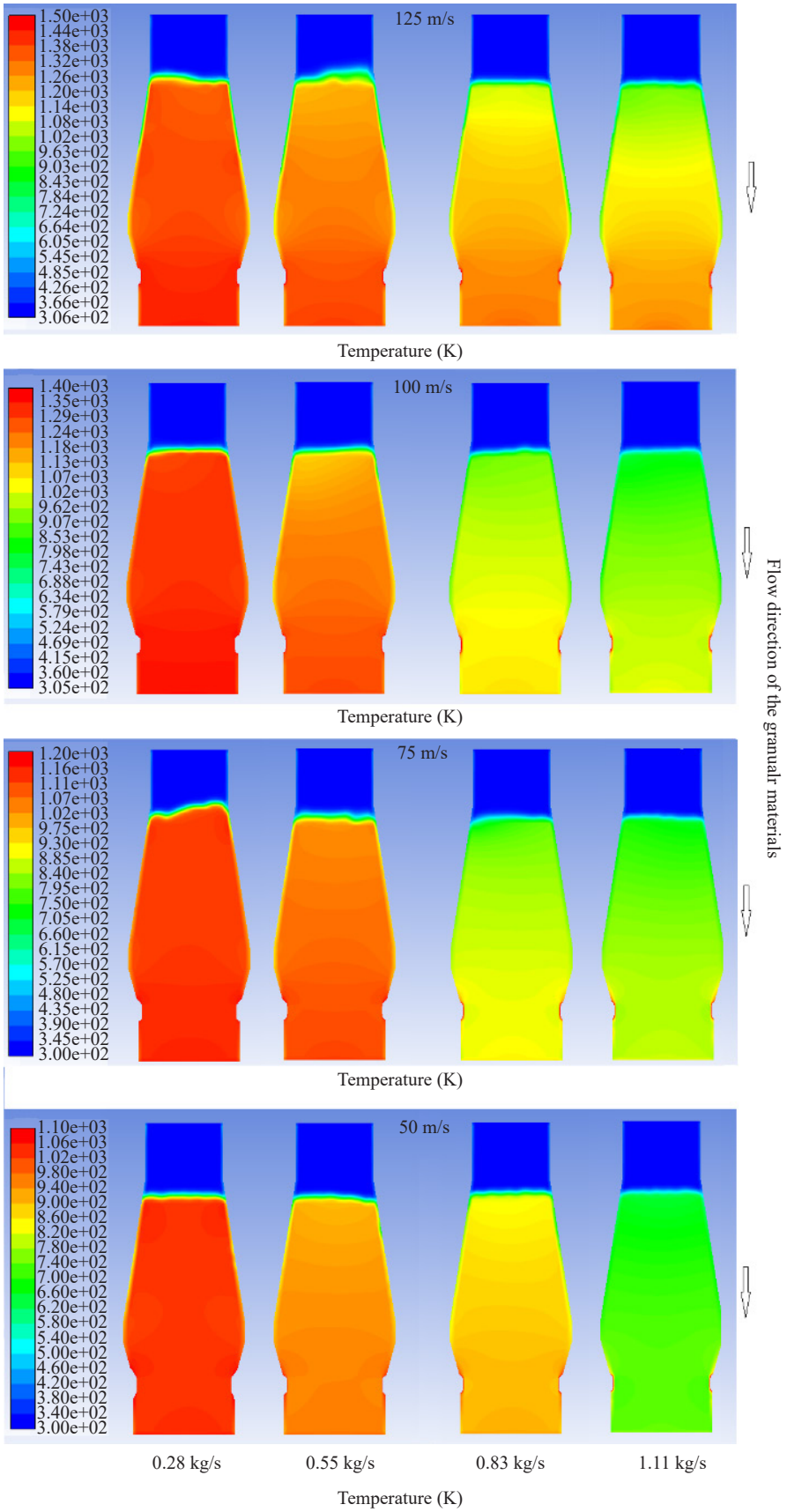

Figure 5. Temperature distribution (K) of granular phase according to the charging rate and blast velocity on the central vertical section

Furthermore, when the mesh size is less than 1.25 cm, i.e., the number of mesh elements is more than 393,024, the difference in pressure loss is not significant. Hence, for further calculations, the number of mesh elements is set to 393,024.

In Figure 4 and 5 the temperature distributions of gas phase and granular phase on the central vertical section are displayed according to the charging rate and blast velocity. Looking at Figure 4, the temperature distribution of the gas is highest near the tuyere and then the gas temperature drops as it rises. It can be seen that the temperature difference increases with the lower blast velocity and the higher charge rate. However, Figure 5 shows that the temperature of the feed does not show a sharp increase in the temperature near the tuyere. This is attributed to the high velocity of the gas in this region, which is responsible for the active convective exchange of the granular medium. When the blast velocity is large and the charge rate is small, the temperature variation of granular material with space position in the furnace is not large in most cases. However, Figure 5 shows that the temperature of granular material in the furnace decreases rapidly when the blast velocity is low and the charging rate is large. It is clear from Figure 4 and 5 that the greater the flow rate of granular material and the smaller the blast velocity, the lower the temperatures in both gas and granular phases. Also the temperature variation in granular phase is not so large but in gas phase it is significantly large. In particular, when blast velocity is 125 m/s and charging rate is more than 0.83 kg/s. Temperature difference between near gas inlet and top of granular bed is about 700 K in gas phase and 200 K in granular phase. It is also shown that as the blast velocity decreases, maximal temperature regions near the inlets are rapidly reduced. Especially, when the blast velocity is 125 m/s, central part of furnace has high temperature but when the blast velocity is small, the heat is not sufficiently transferred to the central part. In Figure 6 and 7 the profiles of temperature on the central axis of furnace are depicted for several values of charging rate and blast velocity. As can be seen from Figure 6, the temperature of gas phase is the highest around the tuyere and again becomes low when going down towards the bottom of furnace. Such a behavior appears most apparently for 125 m/s of the blast velocity. In the granular phase the temperature increases monotonously unlike the gas phase when going down towards the bottom of furnace (See Figure 7). This is because the particles heated at the upper space go down keeping the heat.

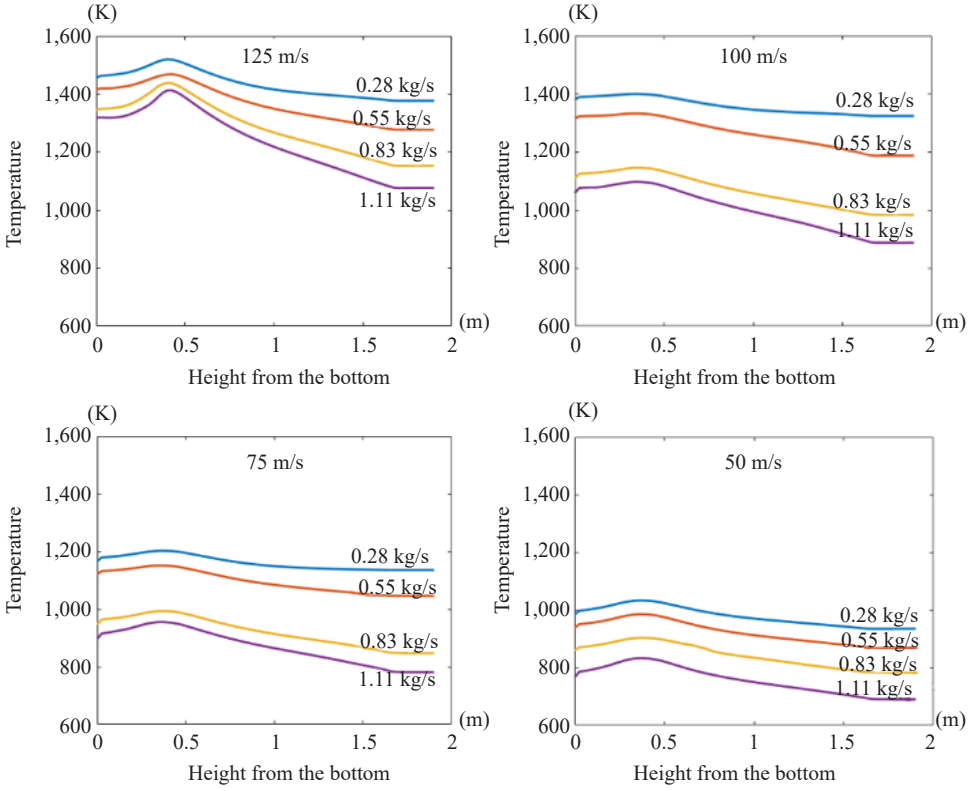

Figure 6. The profiles of temperature of gas phase on the central axis of furnace

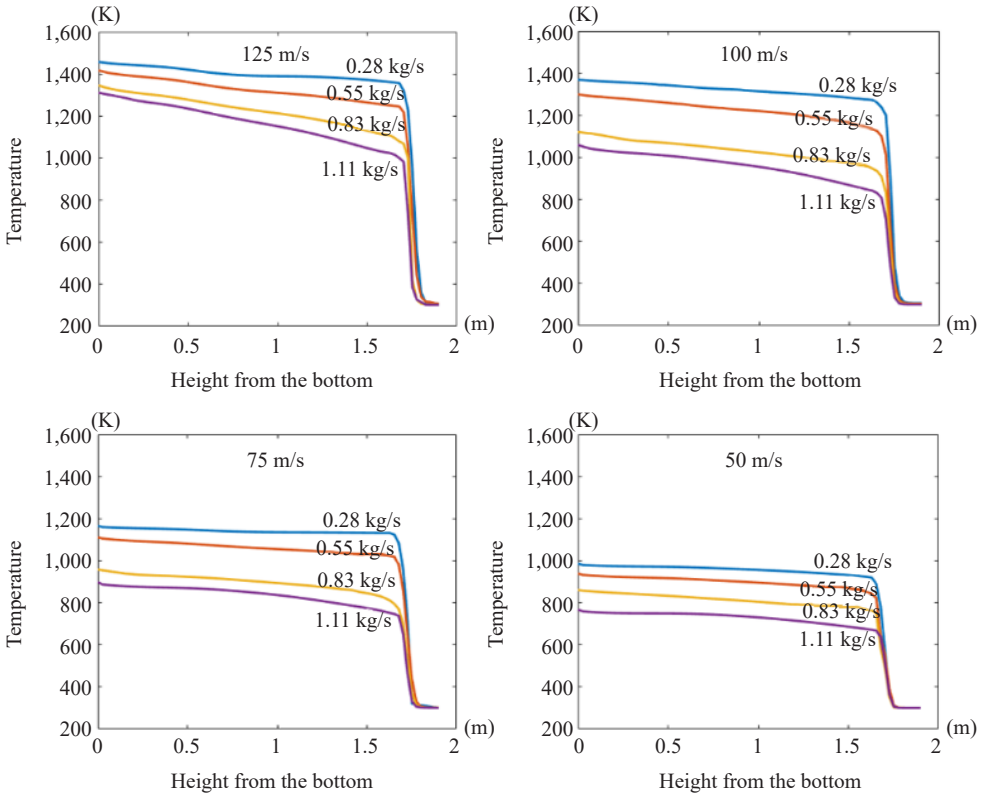

Figure 7. The profiles of temperature of granular phase on the central axis of furnace

Comparison of Figure 6 with Figure 7 shows that both phases have approximately the same temperatures in the lower part of furnace. This shows that the granular material and gas in the range of parameters we consider are in thermal equilibrium in the lower part of the furnace. The most obvious one in Figure 7 is the sharp drop in the temperature distribution of granular material near the free surface. It can be generally thought that the temperature of the granular material layer is reduced at a certain thickness because it takes a certain time for the granular material to heat away from the top. To confirm that the temperature distribution of the granular material at the free surface changed rapidly as such, the temperature variation with time was calculated when one particle of the same particle size and the thermal properties of the material was in the hot gas. The temperature of the hot gas is then given by the temperature of the gas near the free surface shown in Figure 6 and it was calculated how long the particle temperature took to reach the temperature of the granular bed near the free surface shown in Figure 7. The time for the temperature of a single particle to reach the temperature of the granular bed near the free surface was about 60 s~80 s. When the charging rate is large, the time to reach the temperature of the granular bed is short. And the average velocity at which the particle descends can be calculated as follows.

$$\text{The average descending velocity of the particle} = \frac{\text{Charging rate / Density of the particle}}{\text{Cross sectional area in the throat of the furnace}}$$

$$= \frac{\text{Charging rate} / 2,300}{0.22}$$

This value is typically 0.4 mm/s to 2 mm/s. Then, the thickness of the transition layer, which is rapidly rising in temperature near the free surface, is about 3.2 cm to 12 cm. The results of Figure 7 we obtained show that the thickness of this transition layer is slightly thinner, which is presumed to be due to the mixing by boiling of the granular layer near

the free surface.

Additionally, it can be shown from Figure 7 that for charging rate of 0.28 kg/s temperature profile is almost horizontal but for charging rate of 1.11 kg/s its profile has the steeper slope. The temperature difference is evident in the whole region for high particle charging rate and high gas flow rate (see the curves for fan velocity 100 m/s, 125 m/s, granular material loading rate 0.83 kg/s, 1.11 kg/s in Figure 7), but otherwise the temperature difference is not significant in the whole region of the furnace.

This means that the temperature difference between the top and bottom parts of the furnace increases with increasing the charging rate of granular material. Alternatively, let the charging rate be fixed and the blast velocity be varied. As can be seen from Figure 7, the temperature of granular phase doesn't decrease significantly until reaching to the blast velocity of 100 m/s, but its temperature decreases remarkably for the blast velocity below 75 m/s.

As seen from Figure 5, the temperature distributions for some cases have wiggly shape at the granular interface due to boiling of particles.

However, as seen from Figure 8 showing the volume fraction distribution of granular phase, volume fractions at the interface are really small. Here, the top surface of granular bed is horizontal. Also, looking at the case for 125 m/s in Figure 8, there occurs a big gas bubble around each tuyere.

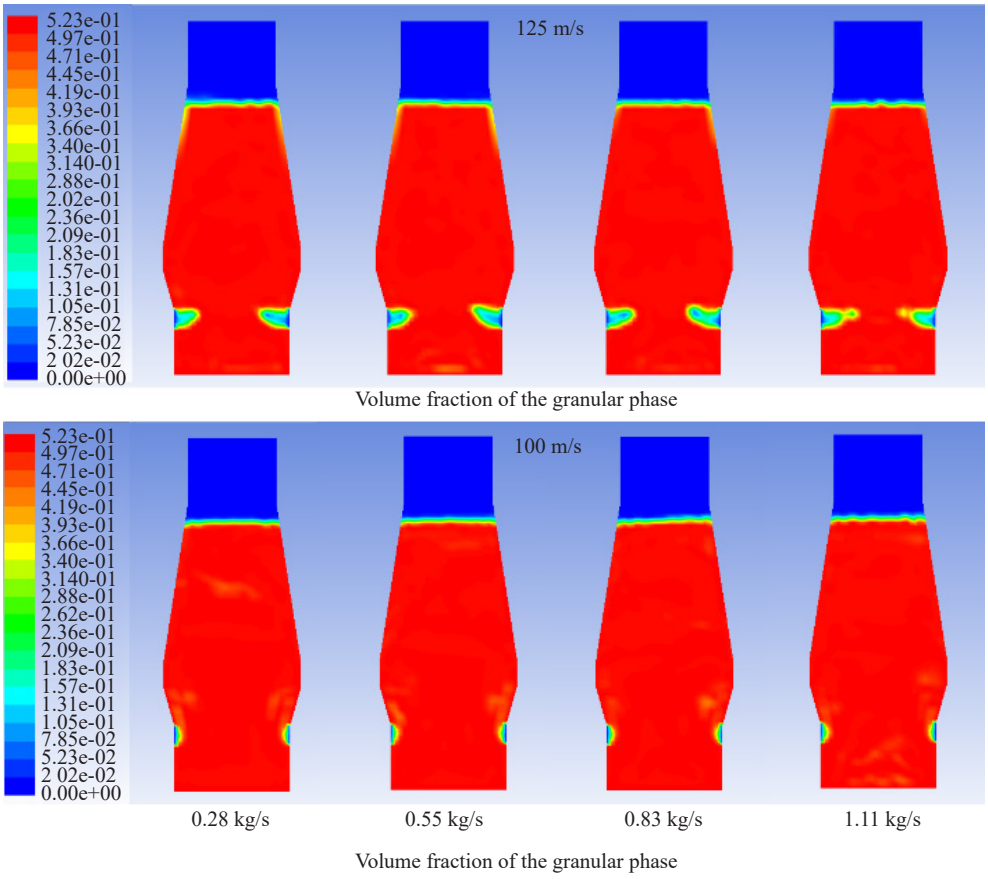

Figure 8. Volume fraction distribution of the granular phase according to the charging rate and blast velocity on the central vertical section

Growth process of gas bubble investigated by transient simulation is as follows: initially, the heated gas injected through the tuyere is cooled and contracted by granular material, so the velocity of gas rapidly decreases and thus size of gas bubble is small. However, because granular material is heated with the time, gas is no longer contracted. As a result, size of gas bubble as well as velocity of gas become great. In particular, for the blast velocity of 100 m/s the gas bubble

formed around the tuyere is very small even in the steady state.

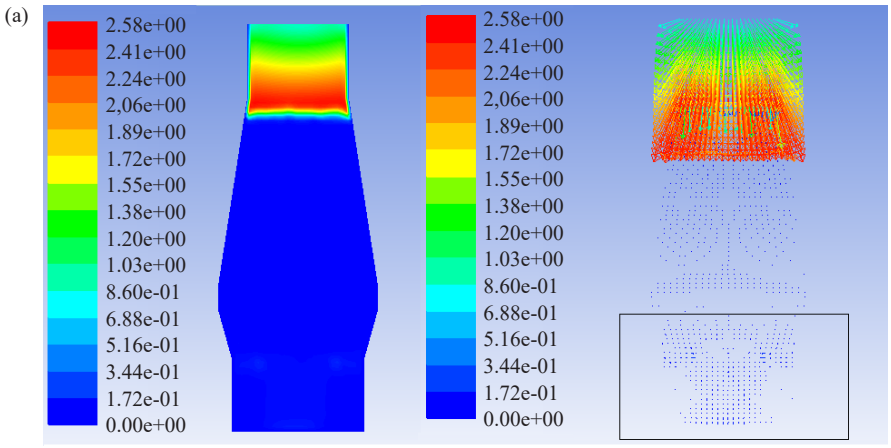

Velocity contour of granular phase Velocity vector of granular phase

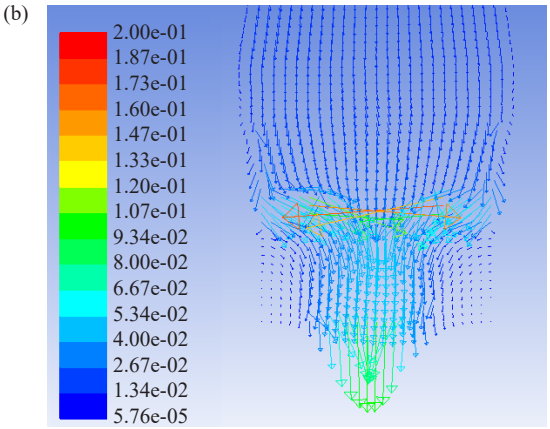

Velocity vector of granular phase (enlargement)

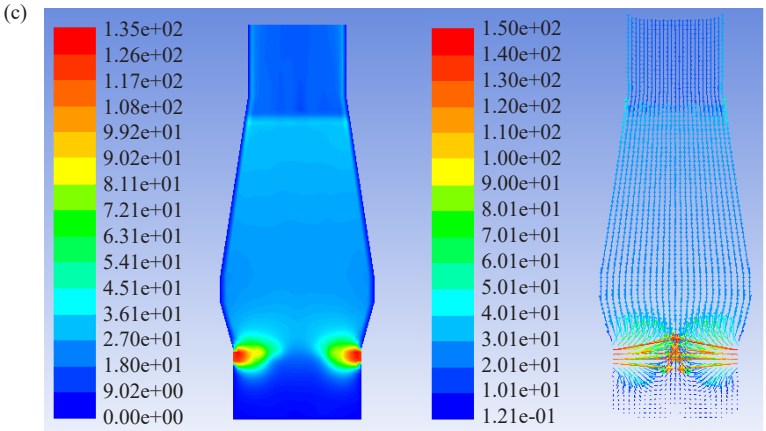

Velocity contour of gas phase Velocity vector of gas phase

Figure 9. Velocity contours and vector distributions for granular and gas phases

Figure 9 shows the velocity contours and vector distributions for both granular and gas phases when the blast velocity is 125 m/s and charging rate is 1.11 kg/s. As seen from velocity contour of granular phase in Figure 9a, the velocity field remains nonzero due to the falling particles in the upper space of furnace but almost zero in the granular bed. From the enlargement figure of velocity vector field of granular phase in Figure 9b, it can be investigated that the particles are discharged at a velocity of about 6 cm/s through the outlet and move at a velocity of 7~8 mm/s elsewhere.

As seen from Figure 9c, gas velocity is fast in the granular bed because gas passage become very narrow due to charged granular material but once escaped from granular bed, it becomes slow. When the blast velocity decreases, flow pattern of gas phase is hardly changed. Here, the heat exchange process between the granular material and the gas is as follows. Figure 9 shows that the heating air enters through the tuyere on both sides below and hits the middle and rises upward. Although there is a pressure that the air is forced to lift, the granular material is heated by air and is lowered by the weight of its own layer. That is, the gas and the particles move in opposite directions, exchanging heat.

As shown in Figure 8, at high blast velocity, bubbles are generated near the tuyere, in which the particle material is actively moving as the packing rate of the particle material is reduced. However, as shown in Figure 9b, the motion of the particles tends to be pushed out of the tuyere and downward. And the granular material continues to heat up as it descends, and the temperature gradually increases.

Figure 10 shows the solid pressure contour for the variation of the feed rate of granular material when the gas blowing rate is 125 m/s. As shown in the figure, when the charging rate of granular material is increased (going to the right in the figure), the region of high solid pressure is widened. As shown in equation (12), the solid pressure will increase as the granular material is compressed, resulting from the maximum packing limit reached. In other words, it means that in the region of high solid pressure, the granular materials become dense.

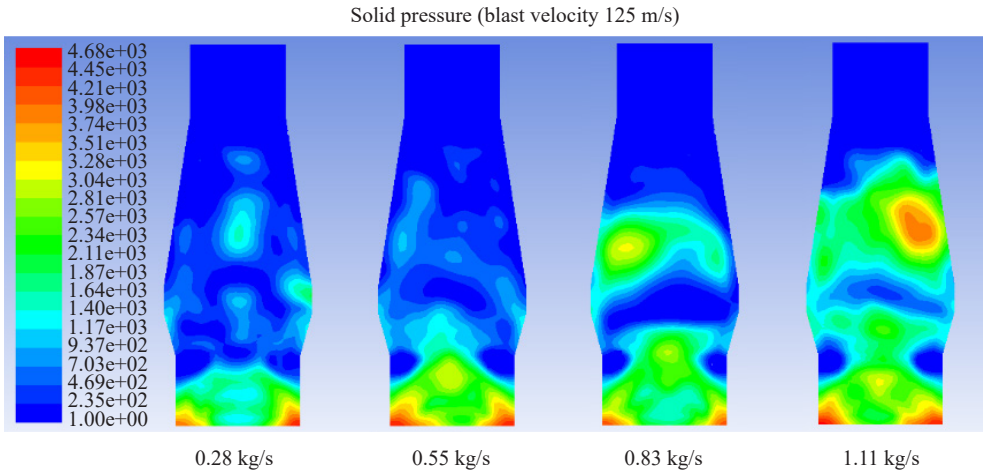

Figure 10. Solid pressure contours with charging rate of the granular material (blast velocity 125 m/s)

The figure shows that the solid pressure distribution is irregular, which continues to change during the unsteady calculation. This shows that the particles are the total downstream flow in the furnace, but that the abnormally local "boiling" occurs and the regions where the solid pressure is small are just such regions. It can be expected that the wider the "boiling" region, the more active the heat exchange in these regions.

Figure 11 shows the solid pressure versus gas blast velocity when the granular material charging rate is 0.28 kg/s. It can be seen that the solid pressure is much lower at 125 m/s than at 50 m/s, and the granular material will descend almost in the compression state at 50 m/s. Also, it can be seen from Figure 10 and 11 that the solid pressure is small near the gas blowing tuyere. That is, in this region, the filling rate of granular material is small and the motion is active.

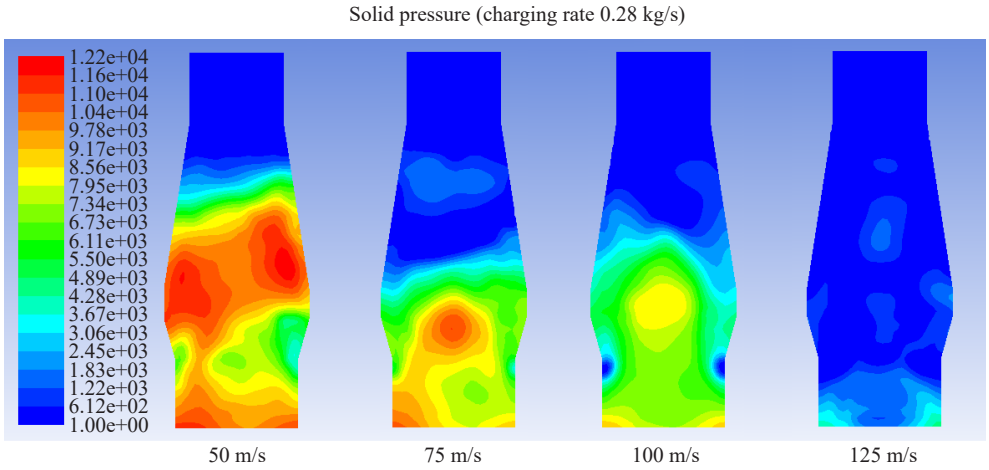

Figure 11. Solid pressure contours with gas blast velocity (charging rate 0.28 kg/s)

On the other hand, we have performed calculations using kinetic theory-based models, i.e., Lun et al., or Syamlal-Obrien model for the solid pressure of the granular phase under above conditions. However, the temperature of the granular phase was not higher than 370 K. This is quite different from the actual phenomenon. This shows that the method based on the assumption of unilateral incompressibility is more suitable for the calculation of the heat transfer process than the model based on kinetic theory in the case of large particle sizes and large density which are not well accompanied in the fluid flow.

If charging rate is zero in our model furnace, the results by non-equilibrium porosity model seem to be comparable with our present model. The blast velocity is 125 m/s and also for other boundaries the same boundary conditions are applied in the calculation by non-equilibrium porosity model. Also Gunn's model (19) and (20) was used for heat transfer coefficient in porosity zone. In this case φ_s is constant in the porosity model but not for the present model.

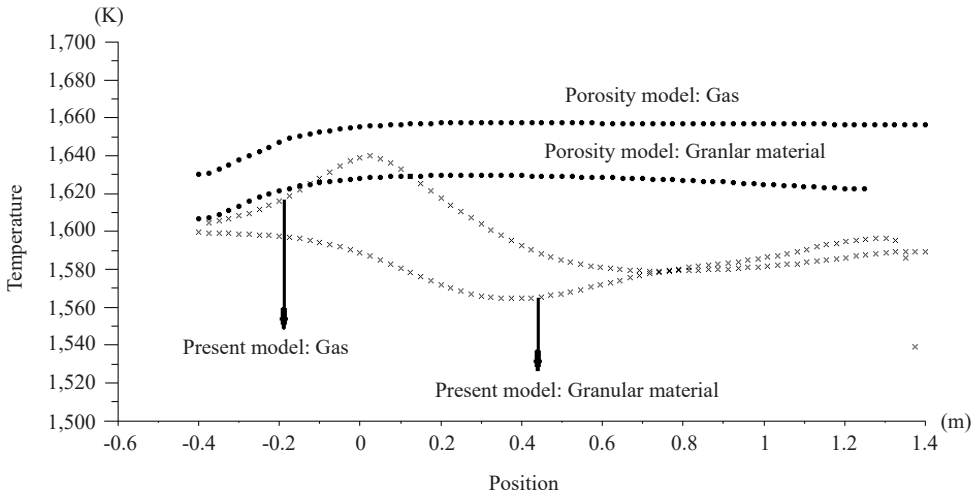

Figure 12. The profiles of temperature of gas phase and granular phase on the central axis of furnace

Figure 12 shows the profiles of temperature of gas phase and granular phase on the central axis of furnace for porosity model and the present model. The porosity model gives the higher temperature than the present model for both of the gas and granular material as seen from Figure 12. It is supposed to result from the fact that thermal energy of the

gas is converted into the motion energy of the granular particles in the present model in contrast to the porosity model. The maximum difference in temperature is about 80 ℃ for the gas and 70 ℃ for the granular material.

Finally, Table 2 shows the comparison between measurements and calculation results for temperature of the granular materials discharged from the outlet of the model furnace. The test for measurement was conducted at the pilot plant of the Institute of Thermal Engineering of the State Academy of Sciences in our country. The temperature was measured by a radiation pyrometer immediately after the particles were exhausted by a scraper discharge device. Particular attention has been paid to maintaining the discharging rate of granular material, the temperature of the heating gas and the inlet flow rate accurately.

Table 2. Comparison between calculation results and measurements for temperature of the discharged granular materials, Cal.: Calculated temperature (℃); Meas.: Measured temperature (℃); Diff.: Absolute difference between calculated and measured values (℃)

Blast velocity	125 m/s			100 m/s			75 m/s			50 m/s		
Charging rate	Cal.	Meas.	Diff.	Cal.	Meas.	Diff.	Cal.	Meas.	Diff.	Cal.	Meas.	Diff.
1.11 kg/s	1,048	1,027	21	805	794	11	614	608	6	508	518	10
0.83 kg/s	1,063	1,057	6	829	835	6	669	673	4	659	637	22
0.55 kg/s	1,139	1,122	17	1,046	1,023	23	860	834	26	668	673	5
0.28 kg/s	1,188	1,161	27	1,113	1,087	26	894	882	12	719	712	7

Also, Figure 13 shows the values of Table 2 visually in the form of a graph. It can be seen from Figure 13 that the temperature difference is large when the inlet charge is changed from 0.83 kg/s to 0.55 kg/s at the blast velocity above 75 m/s. This indicates that the heat exchange is well achieved when the inlet charging rate is less than 0.55 kg/s and the blast velocity is greater than 75 m/s. From the Table 2, it can be seen that calculation results are in agreement with the measured results with maximum absolute error of 27 ℃. Also the Root Mean Square Error (RMSE) absolute error between the experimental and calculated values is 16.4 ℃.

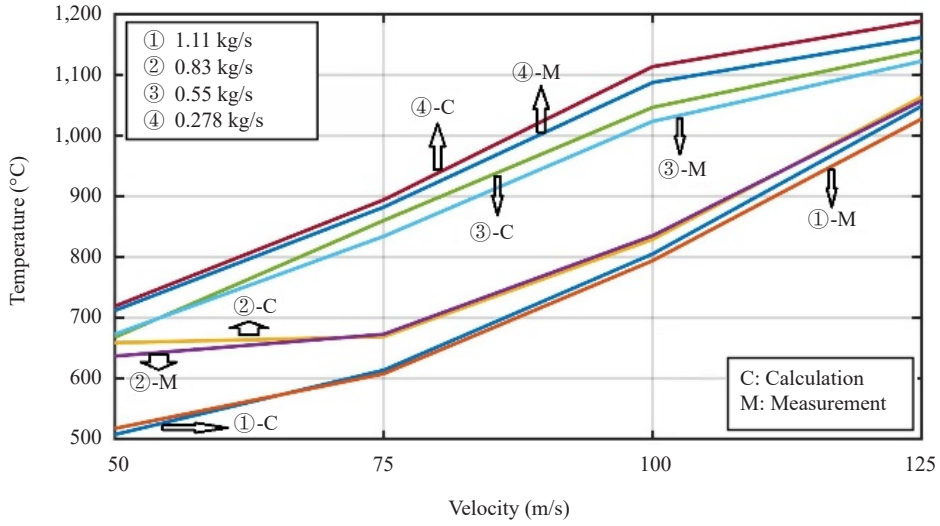

Figure 13. Comparison between calculation results and measurements for temperature of the discharged granular materials

5. Conclusion

In this paper, the previous study[37] for granular flow is extended to the heat transfer problem and applied to the analysis of heat transfer processes in a preheating furnace.

(1) For flows where the particle size is large (> 0.01 m) and the density is high so that the particle does not accompany the flow well, the model assuming the characteristics of the granular medium as unilateral incompressibility is shown to exhibit better behavior than the particle flow model based on kinetic theory.

Indeed, when applying various kinetic theories (e.g., Lun et al., or Syamlal-Obrien model for solid pressure) for granular flow in ANSYS Fluent, the calculation of the temperature distribution in the preheating furnace showed unphysical results in which the maximum temperature did not increase above 370 K under the same conditions as here.

(2) Also the method used for effective heat conductivity of granular materials in DEM was modified in accordance with continuum model.

In order to verify the validity of the model for the contact heat conductivity between particles and convective heat transfer of the granular materials, the comparison with previous work[13] was made. The comparison shows that two results are in good agreement with each other.

(3) Next, thermal characteristics in a model furnace was analyzed, in which dynamic and thermal interaction between fluid and particles as well as heat transfer between particles took place simultaneously.

Thermal change process was considered according to both, charging rate of granular materials and blast velocity in tuyeres. One can know that as charging rate of granular materials increases or blast velocity decreases, the temperature within the preheating furnace is lowered as expected. The temperature distribution of the granular phase and the temperature distribution of the gas phase are quite different. While in the gas phase maximal temperature is reached around tuyeres, in the granular phase the temperature is monotonously increased when going down towards the bottom of furnace.

(4) It was found that the temperature of granular material near the free surface of granular layer increases sharply in the thin transition layer, rather than gradually increasing.

(5) To ensure the temperature of the discharged material is above 1,000 ℃, the inlet charging rate must be less than 0.55 kg/s and the blast velocity above 100 m/s.

When the charging rate of granular materials is zero, the comparison with the non-equilibrium porosity model was made. The porosity model gave the higher temperature than the present model on the central axis for both of the gas and granular material. It was supposed that the reason was due to the conversion of the thermal energy into motion energy of the granular materials in the current approach. Finally, the comparison between measurements and calculation results was made for temperature of the granular materials discharged from the outlet of the model furnace. The result shows that calculation agrees with the measurement comparatively well.

Credit authorship contribution statement

Kum-Song Ku: Conceptualization, Methodology, Writing – original draft, Software, Supervision, Project administrator.

Myong-Il Kim: Conceptualization, Methodology, Writing – review & editing, Investigation, Visualization.

Kwang-Chol Jong: Conceptualization, Writing – review & editing, Validation.

Bok-Chol Song: Conceptualization, Writing – review & editing, Validation.

Conflict of interest

The authors declare that they have no known competing financial interests or personal relationships that could have appeared to influence the work reported in this paper.

References

[1] Cundall, P. A.; Strack, O. D. L. A discrete numerical model for granular assemblies. *Geotech.* **1979,** *29*, 47-65.
[2] Yamane, K.; Nakagawa, M.; Altobelli, S. A.; Tanaka, T. Steady particulate flows in a horizontal rotating cylinder. *Phys. Fluids* **1998,** *10*(6), 1419-1427.
[3] Zhang, S. J.; Yu, A. B.; Zulli, P.; Wright, B.; Austin, P. Numerical simulation of solids flow in a blast furnace. *Appl. Math. Model*. **2002,** *26*, 141-154.
[4] Bluhm-Drenhaus, T.; Simsek, E.; Wirtz, S.; Scherer, V. A coupled fluid dynamic-discrete element simulation of heat and mass transfer in a lime shaft kiln. *Chem. Eng. Sci*. **2010,** *65*, 2821-2834.
[5] Mahmoud, A. E.; Ling, Z.; Weidong, S.; Chen, H.; Ling, B.; Ramesh, A. Theories and applications of CFD-DEM coupling approach for granular flow: A review. *Arch. Comput. Methods Eng*. **2021,** *28*, 4979-5020.
[6] Ling, Z.; Wanning, L.; Ling, B.; Yong, H.; Jian, W.; Weidong, S.; Gaoyang, H. CFD-DEM study of gas-solid flow characteristics in a fluidized bed with different diameter of coarse particles. *Energy Rep*. **2022,** *8*, 2376-2388.
[7] Zhenjiang, Z.; Ling, Z.; Ling, B.; Wanning, L.; Ramesh, K. A. Effects of particle diameter and inlet flow rate on gas−solid flow patterns of fluidized bed. *ACS Omega* **2023,** *8*, 7151-7162.
[8] Yinqiang, S.; Tuo, Z.; Ruiqi, B.; Man, Z.; Hairui, Y. Review of CFD-DEM modeling of wet fluidized bed granulation and coating processes. *Processes* **2023,** *11*, 382.
[9] Zhou, Z. Y.; Zhu, H. P.; Wright, B.; Yu, A. B.; Zulli, P.; Yu, A. B. Gas-solid flow in an iron making blast furnace-II: Discrete particle simulation. *Powder Technol*. **2011,** *208*, 72-85.
[10] Erasmo, S. N.; Alberto, D. R.; Francesco, P. D. M. Coarse graining in discrete element modelling (DEM-CFD) of high solids loading cyclones. *Chem. Eng. Trans*. **2021,** *86*, 1-6.
[11] De Munck, M. J. A.; Peters, E. A. J. F.; Kuipers, J. A. M. Fluidized bed gas-solid heat transfer using a CFD-DEM coarse-graining technique. *Chem. Eng. Sci*. **2023,** *280*, 119048.
[12] Thomas, E.; Nico, J.; Ravindra, A.; Matthias, K. Fluidized bed in industry scale: comparing Eulerian multiphase and coarse-grained CFD-DEM simulation. *Chem. Eng. Trans*. **2023,** *100*, 1-6.
[13] Chaudhuri, B.; Muzzio, F. J.; Tomassone, M. S. Modeling of heat transfer in granular flow in rotating vessels. *Chem. Eng. Sci*. **2006,** *61*, 6348-6360.
[14] Feng, Y. T.; Han, K.; Owen, D. R. J. Discrete thermal element modelling of heat conduction in particle systems: Pipe-network model and transient analysis. *Powder Technol*. **2009,** *193*, 248-256.
[15] Nguyen, V. D.; Cogné, C.; Guessasma, M.; Bellenger, E.; Fortin, J. Discrete modeling of granular flow with thermal transfer: Application to the discharge of silos. *Appl. Therm. Eng*. **2009,** *29*, 1846-1853.
[16] Figueroa, A.; Vargas, W. L.; McCarthy, J. J. Mixing and heat conduction in rotating tumblers. *Chem. Eng. Sci*. **2010,** *65*, 1045-1054.
[17] Zhang, H. W.; Zhou, Q.; Xing, H. L.; Muhlhaus, H. A DEM study on the effective thermal conductivity of granular assemblies. *Powder Technol*. **2011,** *205*, 172-183.
[18] Xie, Q.; Chen, Z.; Mao, Y.; Chen, G.; Shen, W. Case studies of heat conduction in rotary drums with L-shaped lifters via DEM. *Case Stud. Therm. Eng*. **2018,** *11*, 145-152.
[19] Barati, M.; Barati, M.; Peters, B. Coupled CFD-DEM with heat and mass transfer to investigate the melting of a granular packed bed. *Chem. Eng. Sci*. **2018,** *178*, 136-145.
[20] Guo, Z.; Tian, X.; Yang, J.; Shi, T.; Wang, Q. Comparison of heat transfer in gravity-driven granular flow. *J. Therm. Sci*. **2020**, *30*, 441-450.
[21] Guo, Z.; Tian, X. Heat transfer of granular flow around aligned tube bank in moving bed: Experimental study and theoretical prediction by thermal resistance model. *Energy Convers. Manag*. **2022,** *257*, 115435.
[22] Guo, Z.; Tan, Z. Heat transfer prediction of granular flow in moving bed heat exchanger: Characteristics of heat transfer enhancement and dynamic control. *Sol. Energy* **2021,** *230*, 1052-1068.
[23] Tian, X.; Yang, J.; Guo, Z.; Wang, Q. Numerical investigation of gravity-driven granular flow around the vertical plate: Effect of pin-fin and oscillation on the heat transfer. *Energies* **2021,** *14*(8), 2187.
[24] Peter, J. W.; Matthew, D. S.; Paul, W. C.; Philip, M. S. A hierarchical simulation methodology for rotary kilns including granular flow and heat transfer. *Miner. Eng*. **2018,** *119*, 244-262.
[25] Natarajan, V. R.; Hunt, M. L. Kinetic theory analysis of heat transfer in granular flows. *Int. J. Heat Mass Transfer* **1998,** *41*(13), 1929-1944.
[26] Zhang, D. M.; Lei, Y. J.; Yu, B. M.; Pan, G. J. The thermal conductivity theory of non-uniform granular flow and mechanism analysis. *Commun. Theor. Phys*. **2003,** *40*(4), 491-497.
[27] Demagh, Y.; Moussa, H. B.; Lachi, M.; Noui, S.; Bordja, L. Surface particle motions in rotating cylinders:

validation and similarity for an industrial scale kiln. *Powder Technol.* **2012,** *224*, 260-272.
[28] Potgieter, A.; Bhamjee, M.; Kruger, S. Modelling of a heated gas-solid fluidised bed using Eulerian based models. *R & D J. South. Afr. Inst. Mech. Eng*. **2021,** *37*, 45-57.
[29] Jian, P.; Wei, S.; Haisheng, H.; Le, X. CFD modeling and simulation of the hydrodynamics characteristics of coarse coal particles in a 3D liquid-solid fluidized bed. *Minerals* **2021,** *11*, 569.
[30] Schaeffer, D. G. Instability in the evolution equations describing incompressible granular flow. *J. Differ. Equ*. **1987,** *66*, 19-50.
[31] Johnson, P. C.; Jackson, R. Frictional-collisional constitutive relations for granular materials, with application to plane shearing. *J. Fluid Mech*. **1987,** *176*, 67-93.
[32] Rao, K. K.; Nott, P. R. *An Introduction to Granular Flow*; Cambridge University Press: Cambridge, 2008.
[33] Franci, A.; Cremonesi, M. 3D regularized $\mu(I)$-rheology for granular flows simulation. *J. Comput. Phys*. **2019,** *378*, 257-277.
[34] Zheng, Q. J.; Yu, A. B. Modelling the granular flow in a rotating drum by the Eulerian finite element method. *Powder Technol*. **2015,** *286*, 361-370.
[35] Oumaima, E.; Mohamed, L. L.; Bousselham, K. CFD-simulation of gas-solid flow in bubbling fluidized bed reactor. *E3S Web Conf*. **2022,** *336*, 00059.
[36] Narain, R.; Golas, A.; Lin, M. C. Free-flowing granular materials with two-way solid coupling. *ACM Trans. Graph*. **2011,** *30*(5), 1-9.
[37] Ku, K. S.; An, C. H.; Li, K. C.; Kim, M. I. An Eulerian model for the motion of granular material with a large stokes number in fluid flow. *Int. J. Multiph. Flow* **2017,** *92*, 140-149.
[38] Tyliszczak, A.; Szymanek, E. Modeling of heat and fluid flow in granular layers using high-order compact schemes and volume penalization method. *Numer. Heat Transfer, Part A* **2019,** *76*(10), 737-759.
[39] Philipp, B.; Torsten, B.; Stefan, Z. Granular flow field in moving bed heat exchangers: A continuous model approach. *Energy Procedia* **2016,** *99*, 72-79.
[40] Modal, S. S.; Som, S. K.; Dash, S. K. Numerical prediction on the influences of the air blast velocity, inertial bed porosity and bed height on the shape and size of raceway zone in a blast furnace. *J. Phys. D: Appl. Phys*. **2005,** *38*, 1301-1307.
[41] Gidaspow, D. *Multiphase Flow and Fluidization: Continuum and Kinetic Theory Description*; Academic Press: San Diego, 1994.
[42] Li, J.; Kuipers, J. A. M. Gas-particle interactions in dense gas-fluidized beds. *Chem. Eng. Sci*. **2003,** *58*, 711-718.
[43] Zhang, Y.; Reese, J. M. The drag force in two-fluid models of gas-solid flows. *Chem. Eng. Sci*. **2003,** *58*, 1641-1644.
[44] Wright, B.; Zulli, P.; Zhou, Z. Y.; Yu, A. B. Gas-solid flow in an iron making blast furnace—I: Physical modeling. *Powder Technol*. **2011,** *208*, 86-97.
[45] Gunn, D. J. Transfer of heat or mass to particles in fixed and fluidized beds. *Int. J. Heat Mass Transfer* **1978,** *21*, 467-476.
[46] Versteeg, H. K.; Malalasekara, W. *An Introduction to Computational Fluid Dynamics*, 2nd ed.; Pearson Prentice Hall: Harlow, UK, 2007.
[47] Moukalled, F.; Mangani, L.; Darwish, M. *The Finite Volume Method in Computational Fluid Dynamics*; Springer: Cham, 2016.
[48] Cummins, S. J.; Rudman, M. A SPH projection method. *J. Comput. Phys*. **1999,** *152*, 584-607.
[49] Yang, W. J.; Zhou, Z. Y.; Yu, A. B. Discrete particle simulation of solid flow in a three-dimensional blast furnace sector model. *Chem. Eng. J.* **2015,** *278*, 339-352.
[50] Vázquez-Fernández, S.; García-Lengomín Pieiga, A.; Lausín-Gónzalez, C.; Quintela, P. Mathematical modelling and numerical simulation of the heat transfer in a trough of a blast furnace. *Int. J. Therm. Sci*. **2019,** *137*, 365-374.
[51] Yiran, L.; Yansong, S. CFD study of charcoal combustion in a simulated ironmaking blast furnace. *Fuel Process. Technol*. **2019,** *191*, 152-167.
[52] Lin, Q.; Dawei, S.; Yanhui, F.; Haoyan, H.; Xinxin, Z. Study on heat transfer of process intensification in moving bed reactor based on the discrete element method. *Chem. Eng. Process. Process Intensif*. **2020,** *151*, 107915.
[53] Lulu, J.; Shibo, K.; Yuntao, L.; Xiaoming, M.; Hui, X.; Aibing, Y. Numerical simulation of 3D asymmetric inner states of an ironmaking blast furnace resulting from tuyere closure. *Metall. Mater. Trans. B* **2021,** *52*, 2642-2658.
[54] Tao, L.; Guangwei, W.; Heng, Z.; Xiaojun, N.; Cuiliu, Z. Numerical simulation study on the effects of co-injection of pulverized coal and hydrochar into the blast furnace. *Sustainability* **2022,** *14*, 4407.